

ORMDL3-mediated bronchial epithelial pyroptosis leads to lung inflammation in obese mice with asthma

FAN LIU¹⁻³, YAN SUN⁴, YUN ZHOU⁵, YUYE GAO⁴, QIJUN SONG⁴, JIANMEI YANG⁴,
CHAO XU⁶ and GUIMEI LI⁴

¹Children's Hospital Capital Institute of Pediatrics, Chinese Academy of Medical Sciences and Peking Union Medical College; ²Graduate School of Peking Union Medical College;

³Beijing Municipal Key Laboratory of Child Development and Nutriomics, Capital Institute of Pediatrics, Beijing 100020;

⁴Department of Pediatrics, Shandong Provincial Hospital Affiliated to Shandong First Medical University, Jinan, Shandong 250021; ⁵Department of Pediatrics, Shandong Provincial Lanling People's Hospital, Linyi, Shandong 277799;

⁶Department of Endocrinology and Metabolism, Shandong Provincial Hospital Affiliated to Shandong First Medical University, Jinan, Shandong 250021, P.R. China

Received March 20, 2023; Accepted July 20, 2023

DOI: 10.3892/mmr.2023.13073

Abstract. Asthma associated with obesity is a chronic disease that poses a threat to health in children and results in severe wheezing, earlier airway remodeling and increased insensitivity to hormone therapy compared with those who only have asthma. Despite its clinical importance, knowledge on the underlying mechanisms of this disease is limited. The present study aimed to elucidate the pathogenesis of asthma associated with obesity using a murine model. A total of 30 female BALB/c mice were divided into three groups: Normal, mice with asthma and obese mice with asthma. Obese mice with asthma were fed a high-fat diet to induce obesity. Mice with asthma were sensitized and challenged with ovalbumin (OVA). Obese mice were subjected to OVA sensitization and challenge to develop asthma associated with obesity. Airway remodeling was observed in obese mice with asthma through HE and Masson staining. Proteomic and bioinformatics analyses were conducted on lung tissue from obese mice with asthma and normal mice. A total of 200 proteins were differentially expressed in obese mice with asthma compared with normal mice; of these, 53 and 47% were up- and downregulated, respectively. Pathway analysis revealed that asthma associated with obesity primarily affected the 'lysosome', 'phagosome', and 'sphingolipid metabolism' pathways. Gene Set Enrichment Analysis demonstrated the presence of pyroptosis in obese

asthmatic mice, along with significant increases in pyroptosis-associated factors such as GSDMD and Caspase. High protein expression of orosomucoid-like 3 (ORMDL3), NOD-like receptor thermal protein domain associated protein 3 (NLRP3) and Gasdermin-D (GSDMD) was observed in obese mice with asthma. *In vitro* experiments using HBE cells infected with ORMDL3-overexpressing lentivirus demonstrated that the overexpression of ORMDL3 led to increased expression of NLRP3, GSDMD and cathepsin D (CTSD). These findings suggested that ORMDL3 may regulate pyroptosis and subsequent airway remodeling in asthma associated with obesity via the CTSD/NLRP3/GSDMD pathway.

Introduction

Obesity is an independent risk factor for asthma (1). American health survey data show that the incidence of asthma in individuals with obesity is ~11.1% (2). Individuals with obesity have a 1.9-fold higher risk of asthma susceptibility than those without obesity (1). Moreover, >50% of patients with severe asthma are also obese (3). Obesity increases the deposition of collagen fibers, hyperplasia of airway elastin fibers (4) and other ultrastructural airways changes, such as mucous cell hyperplasia (5-9). According to the 2014 Global Asthma Prevention and Treatment Initiative guidelines (10), asthma associated with obesity is a new phenotype of asthma that is associated with poorer asthma control, reduced response to oral corticosteroids and notable decline in lung function. Bronchial epithelial cells (BECs) serve as the first barrier in the airway, protecting against harmful substances and pathogens (11). Cell damage to BECs serves a key role in promoting airway remodeling (12). However, the changes of airway epithelial cells in asthma associated with obesity are not clear.

Pyroptosis is a type of programmed cell death characterized by the involvement of the gasdermin (GSDM) family and is accompanied by the release of proinflammatory cytokines such as interleukin-1 β (IL-1 β) and IL-18.

Correspondence to: Professor Yan Sun, Department of Pediatrics, Shandong Provincial Hospital Affiliated to Shandong First Medical University, 324 Jingwu Weiqi Road, Jinan, Shandong 250021, P.R. China
E-mail: sunyan6150@126.com

Key words: orosomucoid-like 3, pyroptosis, lysosome, asthma, obesity, bronchial epithelial cell

Research has shown that pyroptosis serves a crucial role in respiratory illnesses (13). Exposure to environmental allergens such as *Dermatophagoides farinae* 1 or toluene diisocyanate activates the NOD-like receptor thermal protein domain associated protein 3 (NLRP3)/caspase-1/GSDMD signaling pathway, inducing pyroptosis and resulting in airway inflammation (14,15). A previous study demonstrated that schisandrin B effectively inhibits activation of the NLRP3 inflammasome and decreases pyroptosis via the microRNA-135a-5p/Transient receptor potential canonical type 1 (TRPC1)/STAT3/NF- κ B axis (16). This mechanism mitigates airway inflammation and remodeling in asthma. Furthermore, there are reports indicating that cigarette smoke extract activates the NLRP3/caspase-1/GSDMD signaling pathway, resulting in pyroptosis in BECs, leading to impaired BEC barrier function and severe lung injury (17,18). Obesity increases airway damage in asthma; however, it is unclear whether pyroptosis serves a role or if there is an upstream initiating factor.

In 2007, Moffatt *et al* (19) published genome-wide association research results of asthma for the first time in *Nature* magazine and revealed that ORMDL3 was associated with asthma and other diseases, as well as autophagy and apoptosis (19). A previous study confirmed that ORMDL3 participates in airway remodeling by regulating the ERK/MMP-9/VEGF pathway (20). ORMDL3 belongs to the Orm protein (serum mucoid) family, encodes a transmembrane protein located on the endoplasmic reticulum membrane and regulates sphingomyelin metabolism. High ORMDL3 expression *in vivo* and *in vitro* causes inflammation and promotes ceramide production (21-23). The contribution of ORMDL3 to induction of pyroptosis remains uncertain. The present study aimed to investigate the effect of ORMDL3 on BECs and on the airway remodeling in asthma associated with obesity, as well as to elucidate its underlying mechanisms.

Materials and methods

Animals. A total of 30 female BALB/c mice (age, 4 weeks; weight, 11 \pm 1 g) were obtained from the Experimental Animal Center of Shandong University (Jinan, China). Mice were housed in a controlled environment with a 12/12-h light/dark cycle, maintained at 20-26°C and humidity level of 60-70%. They were provided with ad libitum access to chow and water. Importantly, no mice were prematurely sacrificed during the study. All mice were randomly assigned to three groups: i) Normal [non-sensitized lean (NSL)]; ii) asthmatic (SL) and iii) obese mice with asthma [sensitized obese (SO group)]. NSL and SL groups were fed a standard chow for 14 weeks, while the mice in the SO group received high-fat diet (HFD) containing 60 kcal% for 14 weeks. After 14 weeks of feeding, the SL and SO groups were formed using ovalbumin (OVA) (Fig. 1A), where the mice were sensitized by intraperitoneal (i.p.) injection on days 1 and 8 with 20 μ g OVA (Sigma-Aldrich, Merck KGaA) and 2 mg aluminum hydroxide (Sigma-Aldrich, Merck KGaA) in 200 μ l phosphate-buffered saline (PBS) (19). On days 21-27, mice in SL and SO group were challenged with 1% OVA through ultrasonic atomization for 30 min every day, as previously described (24). Mice in the NSL group received 200 μ l PBS instead of OVA. The study received ethical

approval from the Animal Ethics Committee of Shandong First Medical University (approval no. 2020-1328).

Tissue collection. On day 28 after asthma modelling, mice were euthanized by cervical dislocation following anesthesia with i.p. injection of sodium pentobarbital (35 mg/kg). A total of 50% of the mouse lung tissue was dissected and fresh-frozen in liquid nitrogen before being stored at -80°C until further processing. The rest of the mouse lung tissue was fully fixed using 4% paraformaldehyde solution for 48 h at 4°C for subsequent experiments.

Hematoxylin and eosin (H&E) and Masson staining. The lung tissue was fixed using 4% paraformaldehyde (48 h; 4°C). The lung tissues were embedded in paraffin and cut into 5- μ m thick sections. Subsequently, the paraffin-embedded sections were stained with hematoxylin and eosin (H&E) staining for 5 min and Masson staining for 8 min, both at 37°C. The pathological changes were observed using a light microscope (magnification, x20). IM50 Image Manager software Version 1.20 (Leica Microsystems, Inc.) was used to measure lung pathology changes, including inflammatory situation and collagen deposition. H&E staining was used to investigate inflammatory situation, while Masson staining was used to evaluate collagen deposition in lung tissue. To assess the severity of fibrosis, Szapiel's method (25) was applied using the following scoring system: i) 0, normal tissues without alveolitis or fibrosis; ii) 1, mild alveolitis or fibrosis with \leq 20% lung lesions; iii) 2, moderate alveolitis or fibrosis with 20-50% lung lesions and iv) 3, severe alveolitis or fibrosis with \geq 50% lung lesions. The severity of fibrosis were calculated by reviewing five high-powered fields in every specimen.

Protein extraction and trypsin digestion. Tissue samples were removed storage and an appropriate amount (30 mg) was weighed. Next, samples were subjected to ultrasonic lysis with 300 μ l of SDS lysis solution (Beyotime, China) at a frequency of 1.0 sec on and 1.0 sec off, for a total duration of 3 min on ice at 0°C. The remaining debris was eliminated by centrifugation at 12,000 x g at 4°C for 10 min. The supernatant was collected and the protein concentration was determined using a BCA kit. Trypsin (Beijing Hualishi Tech. Ltd) was added to the protein supernatant for complete enzymolysis once protein concentration was measured. The reaction of enzymolysis was carried out at 37°C for 12 h. Then, peptides were lyophilized. The lyophilized samples were resuspended in 30 μ l 100 mM TEAB and Labeling reaction in a 1.5 ml Eppendorf (EP) tube. 20 μ l acetonitrile were added to TMT reagent and mixed for centrifugation. Then 10 μ l TMT label reagent was added to each sample and incubated for 1 h. Finally, the labeling peptides solutions were lyophilized.

Liquid chromatography-mass spectrometry analysis (LC-MS/MS) and data search. Samples were loaded onto a pre-column Acclaim™ PepMap™ C18 (100 μ m x 2 cm, Thermo Fisher Scientific, Inc.) at a flow rate of 300 nl/min, followed by separation on an analytical column Acclaim™ PepMap™ RSLC (75 μ m x 15 cm, Thermo Fisher Scientific, Inc.). The nitrogen gas temperature was 220°C while the nebulizer pressure was adjusted to 2200 psi. Mass spectrum

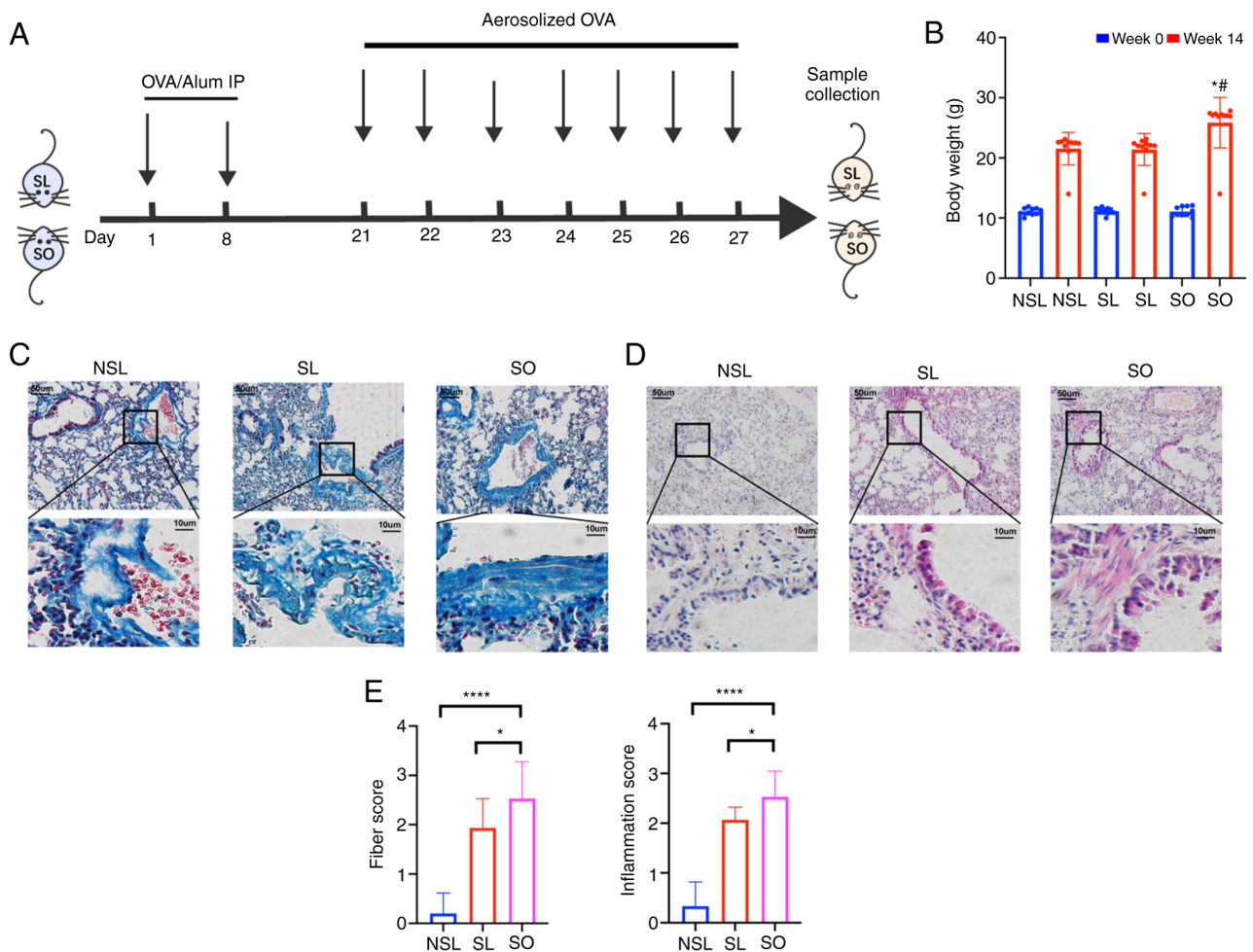


Figure 1. Obesity aggravates airway remodeling and pulmonary inflammation in asthma. (A) Workflow of asthma challenge in mice. (B) Body weight change. (C) Masson and (D) H&E staining of pathological changes in lung tissues. (E) Fibers and inflammation scores showing the morphology of lung sections. * $P < 0.05$, **** $P < 0.0001$ vs. NSL; # $P < 0.05$ vs. SL. NSL, non-sensitized lean; SO, sensitized obese; Alum IP, intraperitoneal aluminum hydroxide.

scanning was conducted at a full scanning mass nucleus ratio in the m/z range of 350-1,500, with MS/MS scanning performed on the 10 highest peaks. All MS/MS spectra were collected under data-dependent positive ionization mode using high-energy collision dissociation, with collision energy set at 30. The resolution of MS was set to 15,000, with automatic gain control set and a maximum injection time of 40 msec. The dynamic exclusion time was 60 sec. The raw data were searched using Proteome Discoverer™ 2.2 (Thermo Fisher Scientific, Inc.) software. The database used for the search was Uniprot *Mus musculus* database (26). False positive rates for peptide identification were controlled at $\leq 1\%$. Specific database search parameter settings are shown in Table I.

Bioinformatics analysis. Principal component analysis (PCA) was performed to assess the differences between the SO and NSL groups based on the expression levels of all proteins (27). Volcano plots were used to show distribution of DEPs between different samples (28). Peptide length distribution analysis was performed to evaluate the conformity of peptide lengths identified by mass spectrometry based on enzymatic hydrolysis and mass spectrometry fragmentation mode (29). Moreover, heatmap was generated to visualize the protein expression patterns in the proteomics study. The heatmap displayed

the relative abundance of proteins across different samples, providing a clear overview of the protein expression levels (30). The clusterProfiler package (version 4.2.2) (31) was used to perform Gene Ontology (GO) (32) and Kyoto Encyclopedia of Genes and Genomes (KEGG) (33) pathway enrichment analyses for differentially expressed proteins (DEPs). To indicate a statistically significant difference, a threshold of fold change ≥ 1.30 or ≤ 0.77 , along with a significance level of $P < 0.05$, was considered. Proteins associated with cell pyroptosis were downloaded from the Gene Set Enrichment Analysis (GSEA; gsea-msigdb.org/gsea/index.jsp; R-MMU-5620971) database. For upregulated proteins in lysosomal pathway, protein-protein interaction (PPI) network was constructed using the Search Tool for the Retrieval of Interacting Genes (STRING; string-db.org/) database with a physical score > 0.132 . Molecular Complex Detection (MCODE) algorithm10 was applied to identify densely connected network components. GSEA was conducted to analyze pyroptosis-associated genes. Marker genes corresponding to each cell type in mouse lung tissue were obtained from the CellMarker database (xteam.xbio.top/CellMarker/) (34).

Immunohistochemical and immunofluorescent staining. The lung tissues were fixed in 4% formalin at room temperature

Table I. Database search parameter settings.

Parameter	Setting
Peptide label	Tandem Mass Tag 6-plex
Cysteine alkylation	Iodoacetamide
Digestion	Trypsin
Instrument	Thermo Scientific™ Q Exactive™ HF
Database	<i>Mus musculus</i> .fasta

for 48 h, followed by paraffin embedding. Serial sections of 5 μ m thickness were cut and used for staining. For immunohistochemical staining, each sections were incubated overnight at 4°C with GSDMD primary antibody (1:1,000; cat. no. ab219800; Abcam). The stained sections were observed under a light microscope (Olympus Corporation, Tokyo, Japan) at a magnification of x100. Five random images per section were collected for analysis.

For immunofluorescent staining, primary antibodies used were ORMDL3 (1:1,000; cat. no. ab211522; Abcam), NLRP3 (1:100; cat. no. ab263899; Abcam). A secondary antibody, Alexa Fluor 488-conjugated goat anti-rabbit/mouse IgM antibody (1:1,000; Life Technologies, Inc.), was used. The sections were then incubated with a 4',6-diamidino-2-phenylindole dihydrochloride (DAPI) solution (1:1,000; Dojindo Laboratories, Inc.) for nuclear staining. Digital section images were captured using an Olympus BX51 imaging system (Olympus Corporation) and quantified with Image-Pro Plus (version 6.0; Media Cybernetics).

Human bronchial epithelial (HBE) cell infected by ORMDL3-overexpressing lentivirus. HBE cells (BEAS-2B) purchased from Shanghai EK-Bioscience Biotechnology Co., Ltd (Shanghai, China). To package ORMDL3-overexpressing lentivirus, ORMDL3 (NM_139280) sequence, GV492 vector, pHelper1.0, and pHelper2.0 (all GeneChem Corporation (Shanghai, China) to synthesize the Ubi-MCS-gcGFP construct. Then, the Ubi-MCS-gcGFP (20 μ g), pHelper1.0 (15 μ g) and pHelper2.0 (10 μ g) were mixed and transfected into 293T cells using GeneChem Transfection kit (GeneChem, Shanghai, China) according to the manufacturer's instructions. After transfection for 48 h at 37°C, the viral supernatants were collected. Subsequently, BEAS-2B were seeded into a six-well dish at 2×10^5 cells/well and then infected with lentiviral vectors loaded with ORMDL3 at an optimum multiplicity of infection (MOI). Following 16 h of infection, the regular culture medium was replaced with fresh medium before subsequent experiments. After 72 h culture at 37°C, expression of the reporter gene was assessed. Cells were collected for downstream experiments when the rate of positive cell infection reached 85% or higher. The group infected with lentivirus overexpressing ORMDL3 can be named as the overexpression (OE) group, while the group infected with empty vector serves as the negative control (NC) group.

Reverse transcription-quantitative PCR (RT-qPCR). Total RNA was extracted from infected HBE using the TRIzol® (Invitrogen; Thermo Fisher Scientific, Inc.). RT was performed

using M-MLV reverse transcriptase Kit (Promega, Fitchburg). RT was performed at 42°C for 1 h, followed by incubation at 70°C for 10 min in a water bath. The expression levels of ORMDL3, GSDMD, NLRP3 and cathepsin D (CTSD) were assessed via RT-qPCR using SYBR Master Mixture (Takara, Canada) according to the manufacturer's protocol. Amplification was performed in following procedure: 95°C for 30 sec, 95°C for 5 sec, and 60°C for 30 sec, for 40 cycles. The threshold cycle of each sample was recorded, and data were analyzed by normalization to GAPDH values using the $2^{-\Delta\Delta C_q}$ method (35). The primer sequences were as follows: ORMDL3, forward 5'-CCT CACCAACCTCATTCACAAC-3' and reverse 5'-TACAGC ACGATGGGTGTGATG-3'; GAPDH, forward 5'-TGACTT CAACAGCGACACCCA-3' and reverse 5'-CACCTGTT GCTGTAGCCAAA-3'; NLRP3, forward 5'-ATGCCCAAG GAGGAAGAG-3' and antisense 5'-CCAACCACAATCTCC GAAT 3'; CTSD, sense 5'-AGGCCCCGTCTCAAAGTA-3' and reverse 5'-ATGCCAATCTCCCCGTAG 3'; GSDMD, forward, 5'-GTGGTTAGGAAGCCCTCAAG-3' and reverse, 5'-CATGGCATCGTAGAAGTGGA 3'; and CTSD forward 5'-AGGCCCCGTCTCAAAGTA-3' and reverse 5'-ATGCCA ATCTCCCCGTAG 3'.

Statistical analysis. Data analysis was performed using GraphPad Prism (version 9.0; Dotmatics) and SPSS (version 27.0; IBM Corp). Data are presented as the mean \pm standard deviation (mean \pm SD) for at least three independent experiments. An Unpaired t-test was used for two-group comparisons. One-way ANOVA was used to assess differences between multiple groups, followed by Dunnett's T3 (when equal variances not assumed) or the Bonferroni's post hoc test (when equal variance was assumed) for pairwise comparisons. $P < 0.05$ was considered to indicate a statistically significant difference.

Results

Airway remodeling is aggravated in asthma associated with obesity. After 14 weeks, weight of the SO group was 20% higher than that of the NSL and SL groups (Fig. 1B). The pathological changes in mouse lung tissue were detected, including inflammatory infiltration and collagen deposition. Masson staining was used to observe collagen deposition. Collagen deposition in the SL and SO groups was significantly higher than that in the NSL group (Fig. 1C and E). The infiltration of monocytes, neutrophils, as well as the shedding of airway epithelial cells, was observed by H&E staining (Fig. 1D). The inflammatory score in the lung tissue of the SO group was increased compared with that of the NSL and SL groups (Fig. 1E). H&E staining can reflect inflammation changes in the lungs, while Masson staining can indicate the presence of collagen deposition. Once lung collagen deposition occurs, it represents irreversible damage, indicating a more severe pathological condition in the lungs. Therefore, Masson staining is of significant importance in assessing lung pathology changes. These results showed that the airway remodeling in obese mice with asthma was the most serious.

Data validation and DEP identification by proteomics. To determine how asthma associated with obesity affected lung

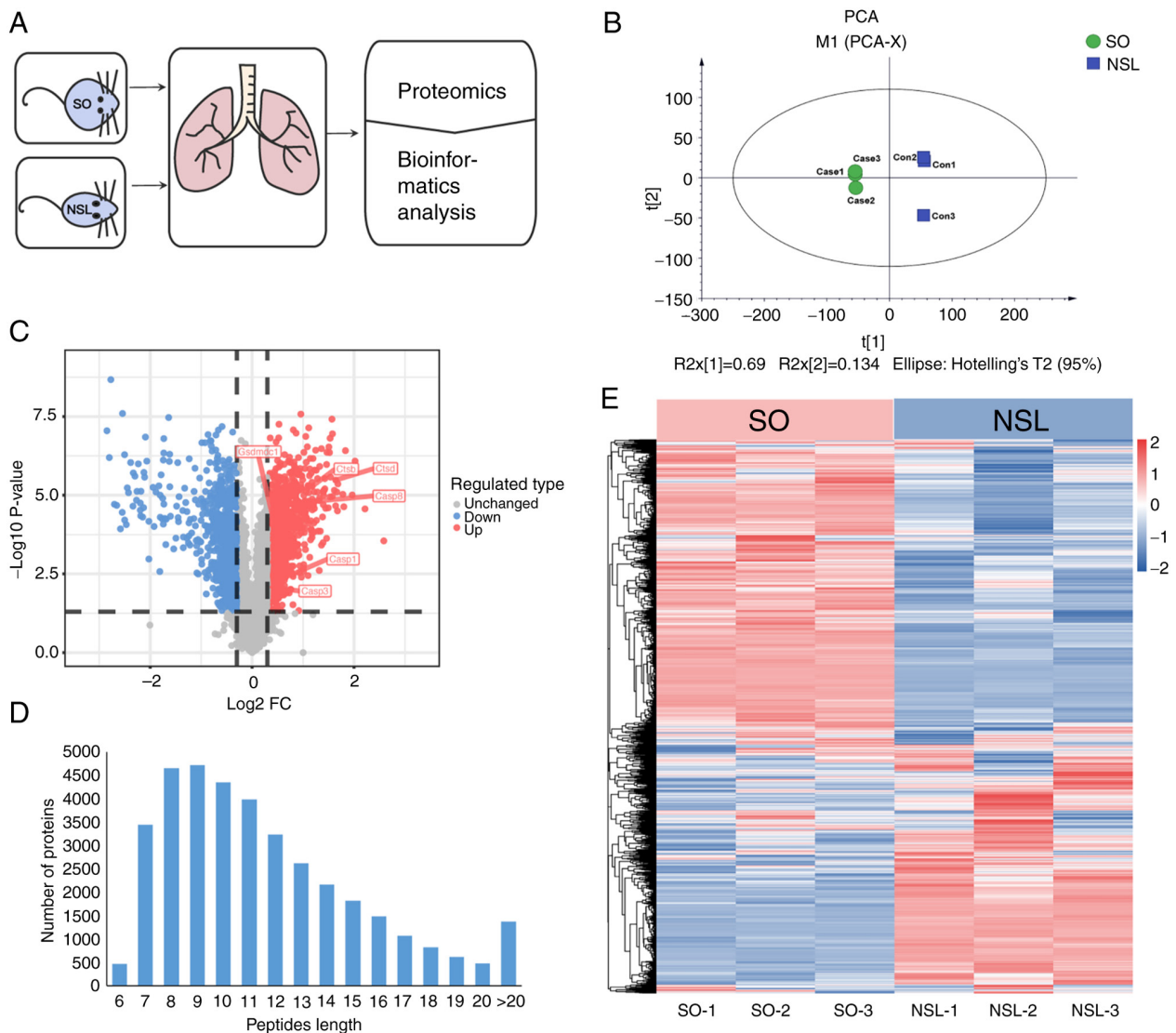


Figure 2. Global proteomics analysis of obese mice with asthma. (A) Proteomics workflow. (B) PCA. (C) Volcano plot showing double thresholds for DEPs in SO and NSL group. Each dot represents a quantified protein. $FC \geq 1.30$ or ≤ 0.50 ; $P < 0.05$. (D) Distribution of peptide length quantified from proteomics data. (E) Heatmap depicting individual samples and protein expression differences ($n=3$). NSL, non-sensitized lean; SO, sensitized obese; PCA, principal Component Analysis; LC-MS/MS, liquid chromatography-mass spectrometry; DEP, differentially expressed protein.

tissue, SO and NSL mouse lung tissues were collected for proteomics (Fig. 2A). PCA was used to validate the dataset. PCA indicated that the six samples from both groups were distinguishable, as shown by short distances between samples in the SO group along PC1 and PC2 and similar distances between samples in the NSL group (Fig. 2B). A total of 6,399 proteins were identified across all groups by proteomics analysis (Table SI). Among these, 5,806 proteins were quantified. Specifically, compared with the NSL group, 823 proteins were upregulated (fold-change >1.3) and 95 proteins were downregulated (fold-change <0.5 ; Fig. 2C; Table SII). The majority of peptides in the 7-20 amino acid range align with the expected pattern from enzymatic hydrolysis and mass spectrometry fragmentation. The identified peptide length distribution meets quality control requirements (Fig. 2D). In Fig. 2E, heatmap analysis showed that the protein expression in SO group mice was altered compared with the NSL group mice, which indicated broad proteome modulation in mouse lungs. Each protein exhibited a distinct concentration

profile, where red and green represented upregulated and downregulated proteins, respectively, while white indicated no significant change in expression levels.

Lysosome and autophagy pathway are enhanced in asthma associated with obesity. To determine the enriched biological processes (BPs), cellular components (CCs) and molecular functions (MFs) of significantly upregulated proteins, GO enrichment analysis was performed (Fig. 3A). Based on P-values obtained through Fisher's exact test, the top three BP terms for upregulated proteins included 'phagocytosis', 'antigen processing and presentation' and 'positive regulation of cell activation'. The top three CCs were 'lytic vacuole', 'lysosome' and 'immunoglobulin complex'. The top three MFs associated with these proteins were 'antigen binding', 'immunoglobulin receptor binding' and 'isomerase activity'. The GO enrichment analysis revealed that the upregulated DEPs were mainly associated with immunity. (Fig. 3B). KEGG pathway enrichment analysis of the identified proteins indicated the

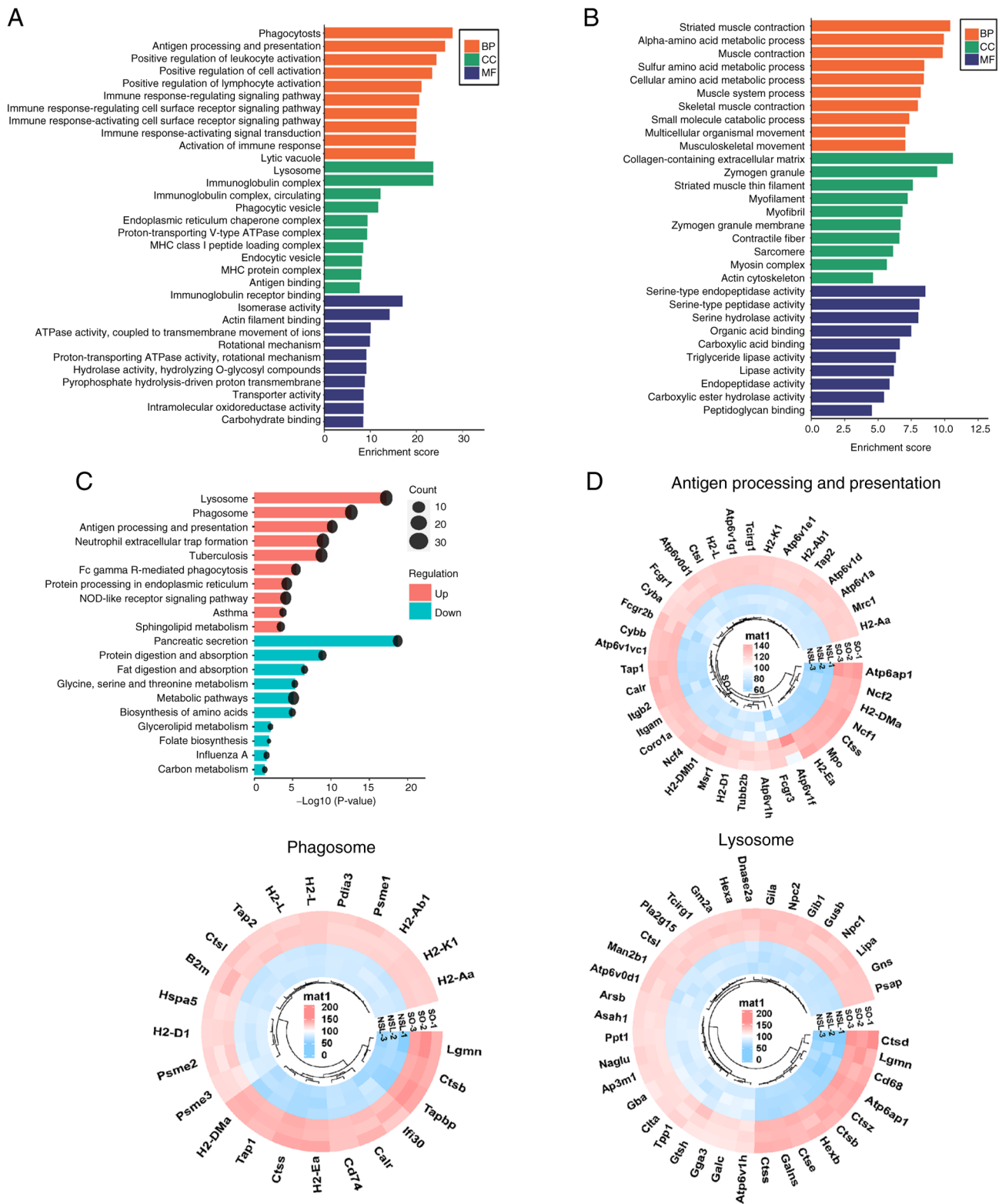


Figure 3. Classification of proteins by GO and KEGG. GO analysis of (A) up- and (B) downregulated DEPs. (C) Distribution of identified DEPs in the KEGG pathway. (D) DEPs in the three most significantly upregulated KEGG pathways were mapped by circular clustering heatmap. GO, Gene Ontology; KEGG, Kyoto Encyclopedia of Genes and Genomes; DEP, differentially expressed protein; BP, biological process; CC, cellular component; MF, molecular function.

involvement of pathways such as ‘Lysosome’, ‘Phagosome’, and ‘Sphingolipid metabolism’ (Fig. 3C; Table SIII). The upregulated pathway-associated genes were clustered in circular heatmaps to display DEPs (Fig. 3D). In the ‘lysosome’ pathway and ‘antigen processing and presentation’ pathway,

CTSD was significantly upregulated in the lung tissue of obese mice with asthma.

Pyroptosis-associated genes are related to lysosomes and metabolism. Using the GSEA database, pyroptosis-associated

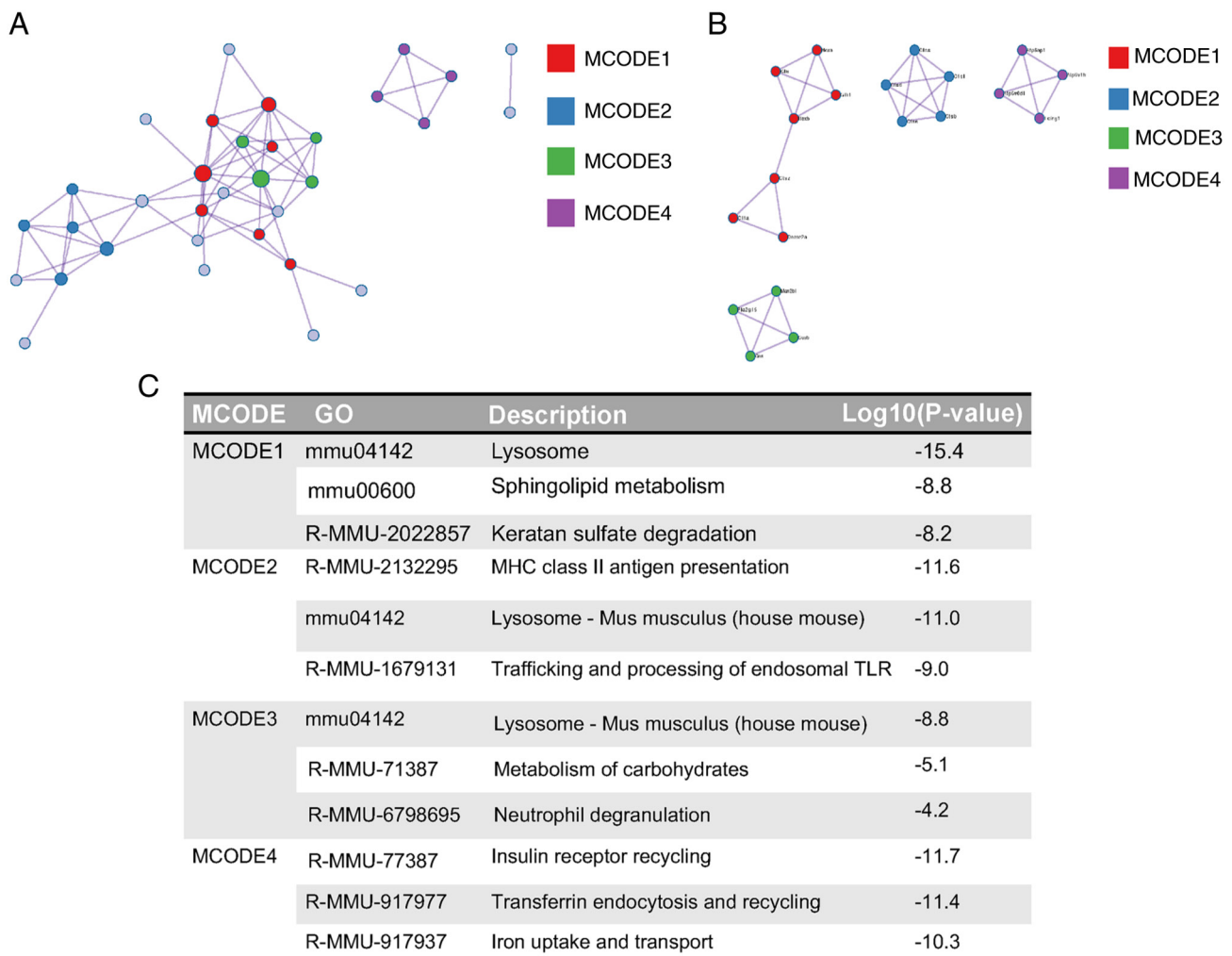


Figure 4. PPI enrichment analysis. (A) Densely connected network components for upregulated proteins in lysosomal pathway. (B) MCODE networks for individual gene lists. (C) Pathway and process enrichment analysis was applied to each MCODE component and the three best-scoring terms by P-value were retained as the functional description of the corresponding components. MCODE, Molecular Complex Detection; PPI, protein-protein interaction; STRING, Search Tool for the Retrieval of Interaction Gene/Proteins; TLR, toll-like receptor; GO, Gene Ontology.

protein information was downloaded, proteins that were not identified by proteomics of the present study were removed and STRING database was used to analyze PPIs (Fig. 4A and B). GO enrichment analysis showed that pyroptosis-associated proteins were associated with lysosomes (Fig. 4C), including CTSD and cathepsin B (CTSB). In addition, MCODE showed that protein was associated with insulin receptors, such as ATPase H⁺ Transporting Accessory Protein 1 and T cell immune regulator 1 (Tcirl). Furthermore, GSEA showed the pyrolytic pathway was notably enhanced (Fig. 5A). The heatmap of pyroptosis-associated genes showed that GSDMD, caspase-1 and -3 and GSDME protein were significantly upregulated (Fig. 5B and C). In addition, PPIs between NLRP3 and pyroptosis-associated proteins were analyzed; NLRP3 interacted with multiple proteins, including caspase-1 and -3, IL-1 β and GSDMD (Fig. 5D). This above interaction pattern suggests that NLRP3 could be involved in the regulation or activation of these pyroptosis-related proteins, indicating its potential role in cell pyroptosis. To identify the specific cell types in the lungs that the upregulated and downregulated differentially expressed proteins (DEPs) were enriched in, we conducted a cell marker analysis. As in Fig. 5E, the upregulated

DEPs were mainly enriched in immune cells and myeloid cells. Conversely, the downregulated DEPs were predominantly enriched in epithelial cells. Interestingly, both the upregulated and downregulated DEPs showed enrichment in macrophages cells (Fig. 5E). This suggests that macrophages play a crucial role in both upregulated and downregulated differentially expressed proteins. They are likely involved in regulating immune responses, inflammation processes, and other related biological functions.

ORMDL3, NLRP3 and GSDMD expression increases in asthma associated with obesity. Immunofluorescence staining showed that expression of ORMDL3 and NLRP3 in the SL and SO groups was increased compared with that in the NSL group (Fig. 6). Immunohistochemical staining showed that levels of GSDMD in the SL and SO groups were increased compared with those in the NSL group (Fig. 6).

CTSD, NLRP3 and GSDMD mRNA expression is increased in HBE cells infected with ORMDL3-overexpressing lentivirus. The fluorescence rate (indicating positive infection rate) was 80% (Fig. 7A). Following infection with

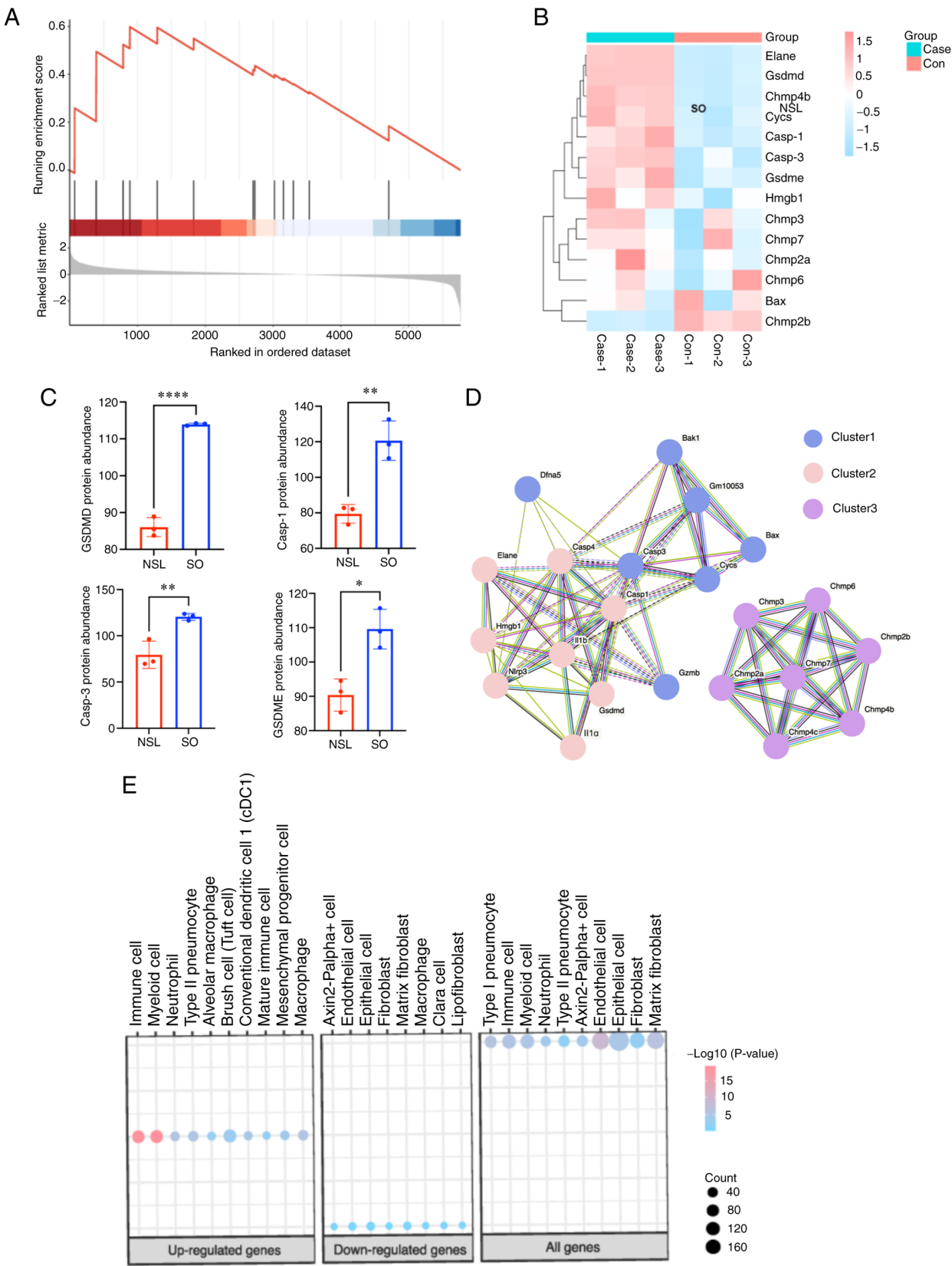


Figure 5. Expression and interaction of pyroptosis-associated proteins. (A) Gene Set Enrichment Analysis of gene set related to cell pyroptosis. (B) Heatmap of pyroptosis-associated genes. (C) Abundance of GSDMD, casp1 and 3 and GSDME peptide. (D) Protein-protein interaction analysis of NLRP3 and pyroptosis-associated genes. (E) Screening of cell types for up- and downregulated DEPs. * $P < 0.05$, ** $P < 0.01$, **** $P < 0.0001$. NSL, non-sensitized lean; SO, sensitized obese; Casp, caspase; GSDMD, Gasdermin D; DEP, differentially expressed protein; NLRP3, NOD-like receptor thermal protein domain associated protein 3.

ORMDL3-overexpressing lentivirus, mRNA expression of ORMDL3, CTSD, NLRP3 and GSDMD was significantly increased in HBE cells compared with the negative controls (Fig. 7B).

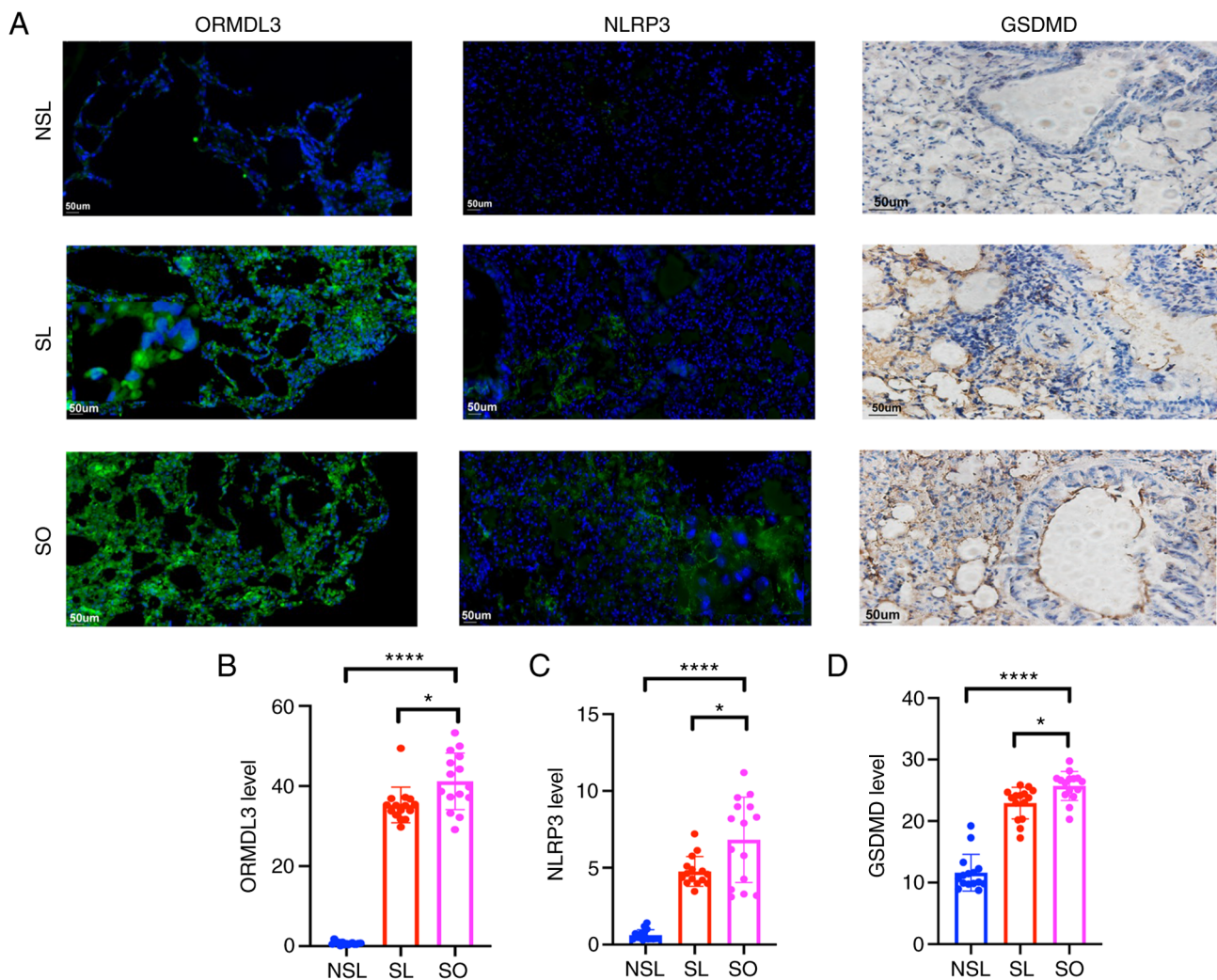


Figure 6. Expression of ORMDL3, NLRP3 and GSDMD. (A) Immunofluorescence and immunohistochemical staining of ORMDL3, NLRP3 and GSDMD. (B) Expression levels of ORMDL3, NLRP3 and GSDMD. * $P < 0.05$, **** $P < 0.0001$. NSL, non-sensitized lean; SO, sensitized obese; GSDMD, gasdermin; NLRP3, NOD-like receptor thermal protein domain associated protein 3; ORMDL3, orosomucoid-like 3.

Discussion

HBE cells serve as the primary barrier in the airway and serve a key role in airway remodeling. Pyroptosis is a proinflammatory cell death process and cell damage pathway that is associated with airway remodeling (36). In the present study, higher expression of ORMDL3 and pyroptosis-associated factors in the lung tissue of obese mice with asthma was observed. ORMDL3 has been shown to participate in airway remodeling in previous study (37). Inflammation and high expression of GSDMD are the hallmarks of pyroptosis (38). The present study indicated that pyroptosis occurred in lung tissue of obese mice with asthma and ORMDL3 and pyroptosis was associated with airway remodeling in asthma associated with obesity.

There has been a growing focus on the role of the NLRP3 inflammasome in asthma (39-41). NLRP3 is the most widely studied member of the NLR family (42,43) and is expressed in the mesenchyme and membrane of neutrophils, macrophages, epithelial cells and other types of cell (43). When stimulated by microbial infection or self-injury signals, the innate immune system inhibits levels of NLRP3, IL-1 β and IL-18, which can

alleviate airway inflammation (44), attenuate airway hyper-responsiveness (45) and effectively prevent progression of asthma (46). NLRP3, an important inflammation factor, is activated in adipose tissue (47). When NLRP3 inflammation is activated, the NLRP3 domain is exposed and NLRP3 oligomerizes to form the NLRP3- apoptosis-associated speck-like protein containing CARD (ASC) complex. Activation of caspase-1, IL-1 β and IL-18, as well as the formation of active N-terminal GSDMD, leads to cell membrane perforation and subsequent release of inflammatory factors. These processes promote cell rupture and induce cell pyroptosis. Pyroptosis is a type of programmed cell death associated with NLRP3 inflammation (48). In this study, NLRP3/GSDMD-associated pyroptosis occurred in obese mice with asthma, which is accompanied by morphological changes in lung tissue. It is likely that the observed morphological alterations in the lung tissue are linked to the inflammatory processes and cellular damage caused by pyroptosis. These findings provide valuable insights into the potential mechanisms underlying the development and progression of obese asthma.

The proteomic results revealed a significant increase in the expression of factors associated with cell pyroptosis.

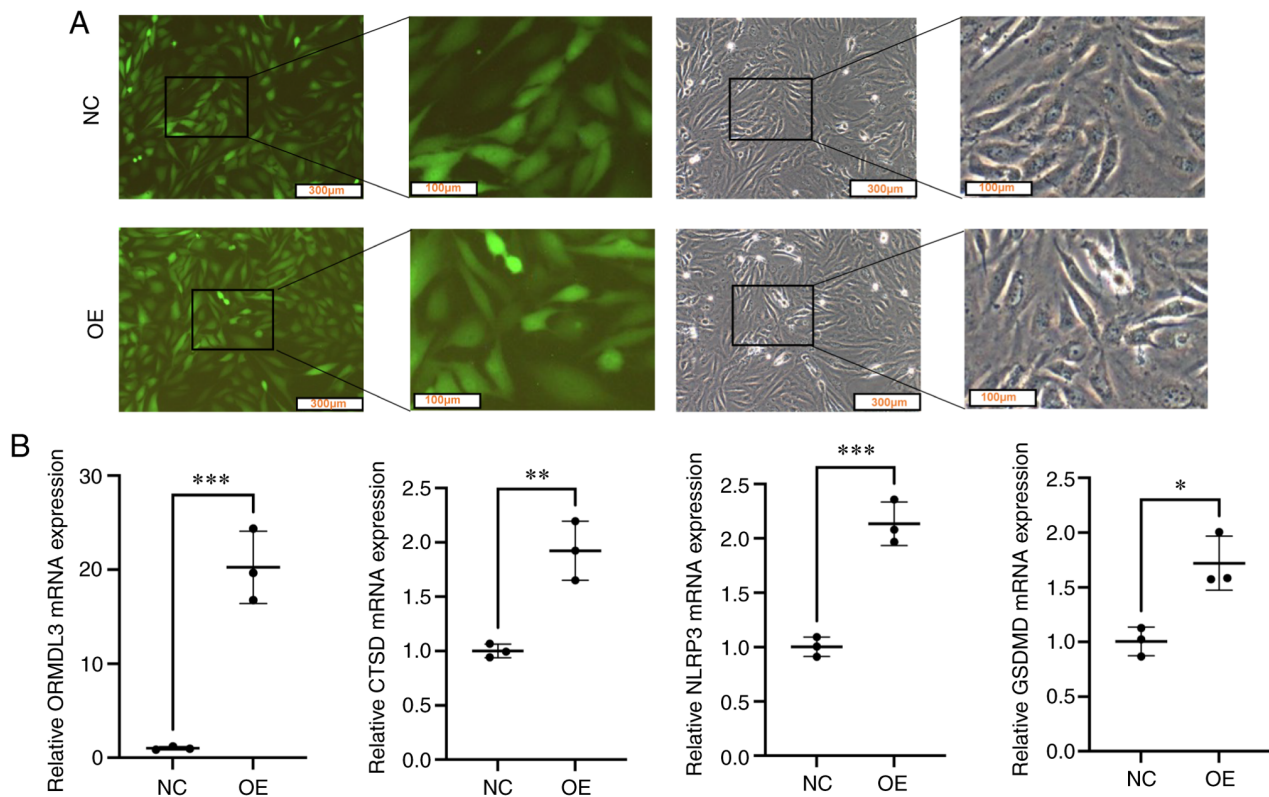


Figure 7. CTSD, NLRP3 and GSDMD mRNA expression in HBE cells infected with ORMDL3-overexpressing lentivirus. (A) HBE cells infected with ORMDL3-overexpressing lentivirus. Scale bar, 100 or 300 μm. (B) CTSD, NLRP3 and GSDMD mRNA expression was detected by reverse transcription-quantitative PCR. * $P < 0.05$, ** $P < 0.01$ and *** $P < 0.001$. NC, negative control; CTSD, cathepsin D; GSDMD, Gasdermin D; NLRP3, NOD-like receptor thermal protein domain associated protein 3; HBE, human bronchial epithelial; OE, overexpression; B, bright field; G, green fluorescence field; ORMDL3, orosomucoid-like 3.

GSEA indicated that the pyroptosis pathway was significantly enhanced. Expression of GSDMD, GSDME and caspase-1 and -3 in the SO group was significantly higher than that in the NSL group. Asthma associated with obesity primarily affected 'lysosome', 'antigen processing and presentation' and 'phagosome', which increased pyroptosis-associated factors, such as GSDMD and GSDME, eventually leading to cell pyroptosis. In addition, immune-associated cells were activated, especially macrophages. Macrophage pyroptosis serves an important role in lung injury and inflammatory diseases, such as sepsis-related acute lung injury (ALI), and Idiopathic pulmonary fibrosis (IPF) (49,50). This suggests that macrophages may serve a vital role via pyroptosis in airway remodeling in asthma associated with obesity. Furthermore, ORMDL3 may influence the biological activity of phagosomes by regulating the related proteins in 'phagosomes' KEGG pathway (Fig. 3C). Caspases, regulators of antioxidant defense and pathogen clearance, primarily regulate phagosomal maturation and fusion with lysosomes (51). Emerging evidence suggests that caspases also contribute to inflammatory cell death by inducing rapid pyroptosis in infected cells (52,53). Based on previous studies, Orm proteins have a direct impact on asthma by regulating sphingomyelin (54,55). In this study, it was observed that asthma with obesity also led to the activation of the 'sphingolipid metabolism' pathway (Fig. 3C), as confirmed by the KEGG pathway analysis. This finding suggests a potential link between the dysregulation of sphingolipid metabolism and the development of asthma with

obesity. Furthermore, it is hypothesized that ORMDL3 may play a critical regulatory role in this potential link.

Sphingolipid are a key family of lipids involved in membrane structure and intracellular signaling. Ceramide serves as a key intermediate product of sphingomyelin metabolism and functions as an inflammatory mediator (56). In obesity, high expression of ORMDL3 *in vivo* and *in vitro* causes inflammation and promotes ceramide production (21,22), especially ceramide $c24:0 > c24:1 > c16:0$ in lung epithelial cells (10). CTSD is a direct downstream factor of ceramide (57). Notably, CTSD belongs to the lysosomal cathepsin family. Entry of CTSD into the cytoplasm increases mitochondrial permeability, releases cytochrome and triggers caspases to induce apoptosis (58). In the present study, CTSD expression was significantly increased in obese mice with asthma. Furthermore, CTSD, NLRP3 and GSDMD expression was increased in HBE cells transfected with ORMDL3-overexpressing lentivirus, which indicated that CTSD may be a link between ORMDL3 and NLRP3/GSDMD-associated pyroptosis. Thus, ORMDL3 may be the initiating factor of pyroptosis. These findings suggested that ORMDL3 may enhance cellular phagocytosis by activating caspases, leading to pyroptosis.

In pyroptosis, CTSD specifically cleaves caspase-8 (59,60) and cleaves and activates GSDMD, leading to the non-classical pyroptosis pathway (61). In addition, caspase-8 can interact with ASC of caspase-1 during bacterial infection, thus activating caspase-1 and the classical pyroptosis pathway. CTSD aggravates the inflammatory reaction in pancreatitis

by enhancing activation of CTSD (62-64). CTSD was found to have pyroptosis-promoting effects (65). Based on the aforementioned results, it was hypothesized that CTSD is associated with pyroptosis of HBE cells in asthma associated with obesity via direct or indirect pathways. Previous study have reported that caspase-1 and -8 play important roles in CTSD-activated pyroptosis (66). In our study, which involved proteome analysis, we also observed an increase of caspase-1 and -8 in asthma associated with obesity. In addition, the present study suggested that ORMDL3 may influence the biological activity of lysosomes. CTSD participated in the lysosomal pathway and was significantly upregulated in lung tissue of obese mice with asthma. Furthermore, HBE cell experiments demonstrated that overexpression of ORMDL3 led to an increase in CTSD expression. ORMDL3 positively regulated pyroptosis-associated factors, including NLRP3 and GSDMD, and pyroptosis-related genes were associated with lysosomes. Although further research is required to understand the mechanisms underlying these observations, the present study suggested that ORMDL3 may play an important role in regulating biological activity of lysosomes.

A limitation of the current study is that it did not investigate protein and mRNA levels of NLRP3, GSDMD and CTSD following transfection with small interfering (si)ORMDL3 to determine the underlying mechanism. The focus of the present study was on the effects of ORMDL3 overexpression and its role in asthma associated with obesity. Further studies are needed to explore the impact of siORMDL3 transfection on the aforementioned protein and mRNA levels.

Overall, the present study indicated that ORMDL3 promoted upregulation of CTSD expression, which led to activation of the NLRP3/GSDMD-related pyroptosis pathway and ultimately contributed to airway remodeling. The present study aimed to elucidate the regulatory mechanism of pyroptosis by ORMDL3 via the CTSD/NLRP3/GSDMD pathway. The present findings provide insight into the underlying mechanisms and may identify therapeutic targets to combat airway remodeling in asthma associated with obesity.

Acknowledgements

Not applicable.

Funding

The present study was supported by the Shandong Provincial Natural Science Foundation (grant no. ZR2020MH003).

Availability of data and materials

The datasets generated and/or analyzed during the current study are available in the ProteomeXchange Consortium repository, proteomecentral.proteomexchange.org (accession no. PXD043630).

Authors' contributions

YS designed the study and edited the manuscript. FL and YZ performed experiments. FL wrote the manuscript. YG, CX, JY, GL and QS analyzed data. FL, YS and QS confirm the

authenticity of all the raw data. All authors read and approved the final manuscript.

Ethics approval and consent to participate

The animal experiments were approved by the Animal Ethics Committee of Shandong Provincial Hospital affiliated with Shandong First Medical University (approval no. 2020-1328) in Shandong, China.

Patient consent for publication

Not applicable.

Competing interests

The authors declare that they have no competing interests.

References

1. Peters U, Dixon AE and Forno E: Obesity and asthma. *J Allergy Clin Immunol* 141: 1169-1179, 2018.
2. Akinbami LJ and Fryar CD: Current asthma prevalence by weight status among adults: United States, 2001-2014. *NCHS Data Brief* 239: 1-8, 2016.
3. Bantula M, Roca-Ferrer J, Arismendi E and Picado C: Asthma and obesity: Two diseases on the rise and bridged by inflammation. *J Clin Med* 10: 169, 2021.
4. Pathak MP, Patowary P, Goyary D, Das A and Chattopadhyay P: β -caryophyllene ameliorated obesity-associated airway hyperresponsiveness through some non-conventional targets. *Phytomedicine* 89: 153610, 2021.
5. Lopes ACR, Zavan B, Corrêa YJC, Vieira TM, Severs LJ, Oliveira LM and Soncini R: Impact of obesity and ovariectomy on respiratory function in female mice. *Respir Physiol Neurobiol* 294: 103775, 2021.
6. Barton JH, Ireland A, Fitzpatrick M, Kessinger C, Camp D, Weinman R, McMahon D, Leader JK, Holguin F, Wenzel SE, *et al*: Adiposity influences airway wall thickness and the asthma phenotype of HIV-associated obstructive lung disease: A cross-sectional study. *BMC Pulm Med* 16: 111, 2016.
7. Gupta S, Lodha R and Kabra SK: Asthma, GERD and obesity: Triangle of inflammation. *Indian J Pediatr* 85: 887-892, 2018.
8. Lamkanfi M and Dixit VM: Mechanisms and functions of inflammasomes. *Cell* 157: 1013-1022, 2014.
9. Cao Y: Angiogenesis and vascular functions in modulation of obesity, adipose metabolism, and insulin sensitivity. *Cell Metab* 18: 478-489, 2013.
10. Reddel HK, Bateman ED, Becker A, Boulet LP, Cruz AA, Drazen JM, Haahtela T, Hurd SS, Inoue H, de Jongste JC, *et al*: A summary of the new GINA strategy: A roadmap to asthma control. *Eur Respir J* 46: 622-639, 2015.
11. Gao W, Li L, Wang Y, Zhang S, Adcock IM, Barnes PJ, Huang M and Yao X: Bronchial epithelial cells: The key effector cells in the pathogenesis of chronic obstructive pulmonary disease? *Respirology* 20: 722-729, 2015.
12. Cohen L, Xueping E, Tarsi J, Ramkumar T, Horiuchi TK, Cochran R, DeMartino S, Schechtman KB, Hussain I, Holtzman MJ, *et al*: Epithelial cell proliferation contributes to airway remodeling in severe asthma. *Am J Respir Crit Care Med* 176: 138-1345, 2007.
13. Liu J, Fan G, Tao N and Sun T: Role of pyroptosis in respiratory diseases and its therapeutic potential. *J Inflamm Res* 15: 2033-2050, 2022.
14. Tsai YM, Chiang KH, Hung JY, Chang WA, Lin HP, Shieh JM, Chong IW and Hsu YL: Der f1 induces pyroptosis in human bronchial epithelia via the NLRP3 inflammasome. *Int J Mol Med* 41: 757-764, 2018.
15. Zhuang J, Cui H, Zhuang L, Zhai Z, Yang F, Luo G, He J, Zhao H, Zhao W, He Y and Sun E: Bronchial epithelial pyroptosis promotes airway inflammation in a murine model of toluene diisocyanate-induced asthma. *Biomed Pharmacother* 125: 109925, 2020.

16. Chen X, Xiao Z, Jiang Z, Jiang Y, Li W and Wang M: Schisandrin B attenuates airway inflammation and airway remodeling in asthma by inhibiting NLRP3 inflammasome activation and reducing pyroptosis. *Inflammation* 44: 2217-2231, 2021.
17. Wang L, Meng J, Wang C, Wang Y, Yang C and Li Y: Hydrogen sulfide attenuates cigarette smoke-induced pyroptosis through the TLR4/NF- κ B signaling pathway. *Int J Mol Med* 49: 56, 2022.
18. Feng Y, Li M, Yangzhong X, Zhang X, Zu A, Hou Y, Li L and Sun S: Pyroptosis in inflammation-related respiratory disease. *J Physiol Biochem* 78: 721-737, 2022.
19. Moffatt MF, Kabesch M, Liang L, Dixon AL, Strachan D, Heath S, Depner M, von Berg A, Bufer A, Rietschel E, *et al*: Genetic variants regulating ORMDL3 expression contribute to the risk of childhood asthma. *Nature* 448: 470-473, 2007.
20. Ding Z, Yu F, Sun Y, Jiao N, Shi L, Wan J and Liu Q: ORMDL3 promotes angiogenesis in chronic asthma through the ERK1/2/VEGF/MMP-9 pathway. *Front Pediatr* 9: 708555, 2021.
21. Song Y, Zan W, Qin L, Han S, Ye L, Wang M, Jiang B, Fang P, Liu Q, Shao C, *et al*: Ablation of ORMDL3 impairs adipose tissue thermogenesis and insulin sensitivity by increasing ceramide generation. *Mol Metab* 56: 101423, 2022.
22. Zhang YM: Orosomucoid-like protein 3, rhinovirus and asthma. *World J Crit Care Med* 10: 170-182, 2021.
23. James B, Milstien S and Spiegel S: ORMDL3 and allergic asthma: From physiology to pathology. *J Allergy Clin Immunol* 144: 634-640, 2019.
24. Kim TB, Kim SY, Moon KA, Park CS, Jang MK, Yun ES, Cho YS, Moon HB and Lee KY: Five-aminoimidazole-4-carboxamide-1- β -D-ribofuranoside attenuates poly (I:C)-induced airway inflammation in a murine model of asthma. *Clin Exp Allergy* 37: 1709-1719, 2007.
25. Wang J, He F, Chen L, Li Q, Jin S, Zheng H, Lin J, Zhang H, Ma S, Mei J and Yu J: Resveratrol inhibits pulmonary fibrosis by regulating miR-21 through MAPK/AP-1 pathways. *Biomed Pharmacother* 105: 37-44, 2018.
26. UniProt Consortium: UniProt: A worldwide hub of protein knowledge. *Nucleic Acids Res* 47: D506-D515, 2019.
27. Metsalu T and Vilo J: ClustVis: A web tool for visualizing clustering of multivariate data using principal component analysis and heatmap. *Nucleic Acids Res* 43: W566-W570, 2015.
28. Cicaloni V, Pecorelli A, Tinti L, Rossi M, Benedusi M, Cervellati C, Spiga O, Santucci A, Hayek J, Salvini L, *et al*: Proteomic profiling reveals mitochondrial alterations in Rett syndrome. *Free Radic Biol Med* 155: 37-48, 2020.
29. Wang S, Zeng Y, He X, Liu F, Pei P and Zhang T: Folate-deficiency induced acyl-CoA synthetase short-chain family member 2 increases lysine crotonylation involved in neural tube defects. *Front Mol Neurosci* 15: 1064509, 2022.
30. Chen G, Cheng J, Yu H, Huang X, Bao H, Qin L, Wang L, Song Y, Liu X and Peng A: Quantitative proteomics by iTRAQ-PRM based reveals the new characterization for gout. *Proteome Sci* 19: 12, 2021.
31. Yu G, Wang LG, Han Y and He QY: clusterProfiler: An R package for comparing biological themes among gene clusters. *OMICS* 16: 284-287, 2012.
32. Qian Z, Cai YD and Li Y: A novel computational method to predict transcription factor DNA binding preference. *Biochem Biophys Res Commun* 348: 1034-1037, 2006.
33. Kanehisa M, Sato Y, Furumichi M, Morishima K and Tanabe M: New approach for understanding genome variations in KEGG. *Nucleic Acids Res* 47: D590-D595, 2019.
34. Zhang X, Lan Y, Xu J, Quan F, Zhao E, Deng C, Luo T, Xu L, Liao G, Yan M, *et al*: CellMarker: A manually curated resource of cell markers in human and mouse. *Nucleic Acids Res* 47: D721-D728, 2019.
35. Livak KJ and Schmittgen TD: Analysis of relative gene expression data using real-time quantitative PCR and the 2(-Delta Delta C(T)) method. *Methods* 25: 402-408, 2001.
36. Liu T, Zhou YT, Wang LQ, Li LY, Bao Q, Tian S, Chen MX, Chen HX, Cui J and Li CW: NOD-like receptor family, pyrin domain containing 3 (NLRP3) contributes to inflammation, pyroptosis, and mucin production in human airway epithelium on rhinovirus infection. *J Allergy Clin Immunol* 144: 777-787, 2019.
37. Yang R, Tan M, Xu J and Zhao X: Investigating the regulatory role of ORMDL3 in airway barrier dysfunction using *in vivo* and *in vitro* models. *Int J Mol Med* 44: 535-548, 2019.
38. de Vasconcelos NM, Van Opdenbosch N, Van Gorp H, Martín-Pérez R, Zecchin A, Vandenabeele P and Lamkanfi M: An apoptotic caspase network safeguards cell death induction in pyroptotic macrophages. *Cell Rep* 32: 107959, 2020.
39. Kim RY, Pinkerton JW, Essilfie AT, Robertson AAB, Baines KJ, Brown AC, Mayall JR, Ali MK, Starkey MR, Hansbro NG, *et al*: Role for NLRP3 inflammasome-mediated, IL-1 β -dependent responses in severe, steroid-resistant asthma. *Am J Respir Crit Care Med* 196: 283-297, 2017.
40. Theofani E, Semitekolou M, Samitas K, Mais A, Galani IE, Triantafyllia V, Lama J, Morianos I, Stavropoulos A, Jeong SJ, *et al*: TFEB signaling attenuates NLRP3-driven inflammatory responses in severe asthma. *Allergy* 77: 2131-2146, 2022.
41. Leszczyńska K, Jakubczyk D and Górka S: The NLRP3 inflammasome as a new target in respiratory disorders treatment. *Front Immunol* 13: 1006654, 2022.
42. Sehgal A, Behl T, Kaur I, Singh S, Sharma N and Aleya L: Targeting NLRP3 inflammasome as a chief instigator of obesity, contributing to local adipose tissue inflammation and insulin resistance. *Environ Sci Pollut Res Int* 28: 43102-43113, 2021.
43. Zhang WJ, Chen SJ, Zhou SC, Wu SZ and Wang H: Inflammasomes and fibrosis. *Front Immunol* 12: 643149, 2021.
44. Guan M, Ma H, Fan X, Chen X, Miao M and Wu H: Dexamethasone alleviate allergic airway inflammation in mice by inhibiting the activation of NLRP3 inflammasome. *Int Immunopharmacol* 78: 106017, 2020.
45. Theofani E, Semitekolou M, Morianos I, Samitas K and Xanthou G: Targeting NLRP3 inflammasome activation in severe Asthma. *J Clin Med* 8: 1615, 2019.
46. Chen S, Yao L, Huang P, He Q, Guan H, Luo Y, Zou Z, Wei S, Peng G, Yan J, *et al*: Blockade of the NLRP3/caspase-1 axis ameliorates airway neutrophilic inflammation in a toluene diisocyanate-induced murine asthma model. *Toxicol Sci* 170: 462-475, 2019.
47. Li Y, Yuan Y, Huang ZX, Chen H, Lan R, Wang Z, Lai K, Chen H, Chen Z, Zou Z, *et al*: GSDME-mediated pyroptosis promotes inflammation and fibrosis in obstructive nephropathy. *Cell Death Differ* 28: 2333-2350, 2021.
48. Bergsbaken T, Fink SL and Cookson BT: Pyroptosis: Host cell death and inflammation. *Nat Rev Microbiol* 7: 99-109, 2009.
49. Jiao Y, Zhang T, Zhang C, Ji H, Tong X, Xia R, Wang W, Ma Z and Shi X: Exosomal miR-30d-5p of neutrophils induces M1 macrophage polarization and primes macrophage pyroptosis in sepsis-related acute lung injury. *Crit Care* 25: 356, 2021.
50. Liang Q, Cai W, Zhao Y, Xu H, Tang H, Chen D, Qian F and Sun L: Lycorine ameliorates bleomycin-induced pulmonary fibrosis via inhibiting NLRP3 inflammasome activation and pyroptosis. *Pharmacol Res* 158: 104884, 2020.
51. Songane M, Khair M and Saleh M: An updated view on the functions of caspases in inflammation and immunity. *Semin Cell Dev Biol* 82: 137-149, 2018.
52. Achoui Y, Leaf IA, Hagar JA, Fontana MF, Campos CG, Zak DE, Tan MH, Cotter PA, Vance RE, Aderem A and Miao EA: Caspase-11 protects against bacteria that escape the vacuole. *Science* 339: 975-978, 2013.
53. Miao EA, Rajan JV and Aderem A: Caspase-1-induced pyroptotic cell death. *Immunol Rev* 243: 206-214, 2011.
54. Debeuf N, Zhakupova A, Steiner R, Van Gassen S, Deswarte K, Fayazpour F, Van Moorlegheem J, Vergote K, Pavie B, Lemeire K, *et al*: The ORMDL3 asthma susceptibility gene regulates systemic ceramide levels without altering key asthma features in mice. *J Allergy Clin Immunol* 144: 1648-1659, 2019.
55. Breslow DK, Collins SR, Bodenmiller B, Aebersold R, Simons K, Shevchenko A, Ejsing CS and Weissman JS: Orm family proteins mediate sphingolipid homeostasis. *Nature* 463: 1048-1053, 2010.
56. Jannet AH and Ogretmen B: Targeting sphingolipid metabolism as a therapeutic strategy in cancer treatment. *Cancers (Basel)* 14: 2183, 2022.
57. Heinrich M, Wickel M, Schneider-Brachert W, Sandberg C, Gahr J, Schwandner R, Weber T, Saftig P, Peters C, Brunner J, *et al*: Cathepsin D targeted by acid sphingomyelinase-derived ceramide. *EMBO J* 18: 5252-5263, 1999.
58. Bhadra K: A mini review on molecules inducing caspase-independent cell death: A new route to cancer therapy. *Molecules* 27: 6401, 2022.
59. Conus S, Pop C, Snipas SJ, Salvesen GS and Simon HU: Cathepsin D primes caspase-8 activation by multiple intra-chain proteolysis. *J Biol Chem* 287: 21142-21151, 2012.
60. Di YQ, Han XL, Kang XL, Wang D, Chen CH, Wang JX and Zhao XF: Autophagy triggers CTSD (cathepsin D) maturation and localization inside cells to promote apoptosis. *Autophagy* 17: 1170-1192, 2021.

61. Orning P, Weng D, Starheim K, Ratner D, Best Z, Lee B, Brooks A, Xia S, Wu H, Kelliher MA, *et al*: Pathogen blockade of TAK1 triggers caspase-8-dependent cleavage of gasdermin D and cell death. *Science* 362: 1064-1069, 2018.
62. Aghdassi AA, John DS, Sandler M, Weiss FU, Reinheckel T, Mayerle J and Lerch MM: Cathepsin D regulates cathepsin B activation and disease severity predominantly in inflammatory cells during experimental pancreatitis. *J Biol Chem* 293: 1018-1029, 2018.
63. Xing Y, Wang JY, Li MY, Zhang ZH, Jin HL, Zuo HX, Ma J and Jin X: Convallatoxin inhibits IL-1 β production by suppressing zinc finger protein 91 (ZFP91)-mediated pro-IL-1 β ubiquitination and caspase-8 inflammasome activity. *Br J Pharmacol* 179: 1887-1907, 2022.
64. Song Z, Zou J, Wang M, Chen Z and Wang Q: A comparative review of pyroptosis in mammals and fish. *J Inflamm Res* 15: 2323-2331, 2022.
65. Liu C, Yao Q, Hu T, Cai Z, Xie Q, Zhao J, Yuan Y, Ni J and Wu QQ: Cathepsin B deteriorates diabetic cardiomyopathy induced by streptozotocin via promoting NLRP3-mediated pyroptosis. *Mol Ther Nucleic Acids* 30: 198-207, 2022.
66. Chen S, Zhou C, Yu H, Tao L, An Y, Zhang X, Wang Y, Wang Y and Xiao R: 27-Hydroxycholesterol contributes to lysosomal membrane permeabilization-mediated pyroptosis in co-cultured SH-SY5Y cells and C6 cells. *Front Mol Neurosci* 12: 14, 2019.



Copyright © 2023 Liu et al. This work is licensed under a Creative Commons Attribution-NonCommercial-NoDerivatives 4.0 International (CC BY-NC-ND 4.0) License.